

Phase control and lateral heterostructures of MoTe₂ epitaxially grown on graphene/Ir(111)

Joan Ripoll-Sau, Fabian Calleja, Pablo Casado Aguilar, Iván M. Ibarburu, Amadeo L. Vázquez de Parga, Rodolfo Miranda and Manuela Garnica

This is the accepted version of the following article: Joan Ripoll-Sau, Fabian Calleja, Pablo Casado Aguilar, Iván M. Ibarburu, Amadeo L. Vázquez de Parga, Rodolfo Miranda and Manuela Garnica. Phase control and lateral heterostructures of MoTe₂ epitaxially grown on graphene/Ir(111), *Nanoscale* 2022, which has been published in final form at <https://doi.org/10.1039/D2NR03074H>.

To cite this version

Joan Ripoll-Sau, Fabian Calleja, Pablo Casado Aguilar, Iván M. Ibarburu, Amadeo L. Vázquez de Parga, Rodolfo Miranda and Manuela Garnica. Phase control and lateral heterostructures of MoTe₂ epitaxially grown on graphene/Ir(111), *Nanoscale* 2022. <https://repositorio.imdeananociencia.org/handle/20.500.12614/3140>

Licensing

See RSC Terms & Conditions <https://www.rsc.org/journals-books-databases/librarians-information/products-prices/licensing-terms-and-conditions/>

Embargo

This version (post-print or accepted manuscript) of the article has been deposited in the Institutional Repository of IMDEA Nanociencia with an embargo lifting on 08.07.2023.

Phase control and lateral heterostructures of MoTe₂ epitaxially grown on graphene/Ir(111)

Joan Ripoll-Sau^{a,b}, Fabian Calleja^a, Pablo Casado Aguilar^{a,b},
Iván M. Ibarburu^{a,b}, Amadeo L. Vázquez de Parga^{a,b,c,d},
Rodolfo Miranda^{a,b,c,d}, Manuela Garnica^{a,c}

^a Instituto Madrileño de Estudios Avanzados en Nanociencia (IMDEA-Nanociencia),
28049 Madrid, Spain

^b Departamento de Física de la Materia Condensada, Universidad Autónoma de
Madrid, 28049 Madrid, Spain

^c Instituto "Nicolás Cabrera", Universidad Autónoma de Madrid, 28049 Madrid,
Spain

^d Condensed Matter Physics Center (IFIMAC), Universidad Autónoma de Madrid,
28049 Madrid, Spain

E-mail: manuela.garnica@imdea.org

Abstract. Engineering the growth of the different phases of two-dimensional transition metal dichalcogenides (2D-TMDs) is a promising way to exploit their potential since the phase determines their physical and chemical properties. Here, we report on the epitaxial growth of monolayer MoTe₂ on graphene on an Ir(111) substrate. Scanning tunneling microscopy and spectroscopy provide insights into the structural and electronic properties of the different polymorphic phases, which remain decoupled from the substrate due to the weak interaction with graphene. In addition, we demonstrate a great control of the relative coverage of the relevant 1T' and 1H MoTe₂ phases by varying the substrate temperature during the growth. In particular, we obtain large areas of the 1T' phase exclusively or the coexistence of both phases with different ratios.

1. Introduction

Two-dimensional (2D) transition metal dichalcogenides (TMDs) are layered compounds with a stoichiometry of MX₂, where M is a transition metal element (groups IV-X) and X is a chalcogen element (mainly S, Se or Te). They show a wide range of physical properties from semimetallic to semiconductors, superconductors or insulators, changing even between materials with the same composition but different crystalline phases. In the last years, 2D-TMDs have demonstrated a great potential in a wide range of areas ranging from opto-electronics and catalysis to energy storage or quantum electronics [1, 2, 3, 4]. However, the implementation of 2D-TMDs with a stable semiconducting behaviour in electronic devices has been hampered by the Schottky contact between

the metal electrode and the 2D material. To avoid this issue, a smart solution based in a lateral heterophase structure of the same TMD has been proposed [5, 6]. The idea consists in the fabrication of a homojunction with a semiconducting phase as channels and a metallic phase of the same material as electrodes, thus producing an ohmic contact. A promising candidate to this aim is MoTe_2 , which, contrary to other tellurides, such as WTe_2 , exhibits two phases stable at 300 K with the appropriate properties. On the one side, the 2H phase of MoTe_2 is a semiconductor with a hexagonal structure, which shows a direct bandgap at the monolayer (the so-called 1H phase) [7, 8] that evolves into an indirect bandgap (1.0-1.3 eV) at the multilayer regime [9]. On the other hand, the bulk 1T' phase is metallic and suffers a structural phase transition to a three dimensional topological Weyl semimetal Td phase at 240 K [10] and is predicted to host quantum spin hall (QSH) states in the monolayer regime [3]. However, controversial results have been reported regarding the opening of a positive QSH gap [11, 10]. Interestingly, it has been demonstrated that due to the small energy difference between phases, the 1H phase can be transformed into the 1T' phase by strain or laser irradiation [5, 11]. Phase control in MoTe_2 has then emerged as an interesting approach to the fabrication of heterophase homojunctions with multiple applications [6, 12].

Most of the results regarding phase engineering in TMDs have been obtained for bulk crystals. For instance, single crystals of 2H- MoTe_2 , synthesized using the flux method, were directly transformed into the 1T' phase at temperatures higher than 770 K [10] and later mechanically exfoliated [3]. However, no regular 1T'- MoTe_2 phase was obtained by this approach. In addition, whereas the quality of the layers is suitable for fundamental research, the thickness inhomogeneities, high defect density and uneven interfaces obtained by this technique are still jeopardizing applications [9, 13]. Epitaxial growth of 2D materials on a variety of substrates has been demonstrated to be scalable to large-area production with a better control of thickness and structural quality of the layers [14], even creating vertical TMDs heterostructures with sharp interfaces in a controlled atmosphere [15]. In spite of the low chemical reactivity of Mo with Te, few-layer films of MoTe_2 were successfully synthesized by tellurization of Mo thin films via Te sublimation [16] and chemical vapor deposition (CVD) [17]. As an alternative, molecular beam epitaxy (MBE) has been used to grow 2H- MoTe_2 thin films on graphene on 6H-SiC(0001) [18], SiO_2 [19], GaAs(111)B[20], CaF_2 [21], InAs(111)/Si(111) [22] and c- Al_2O_3 (0001) [23], although the small grain size of the grown layer results in poor transport properties [23]. Besides, the formation of a single MoTe_2 layer with different stoichiometry and diverse physical properties has been reported on highly oriented pyrolytic graphite (HOPG) [24, 25, 26], bilayer of graphene on SiC (BLG/SiC) [26, 27] and MoS_2 [28]. However, the production of large domains of metallic 1T' phase or the control of the fabrication of heterophase structures are still challenging, as a result of both the tendency of Te to desorb from the surface during the growth process and the small energy difference between the 1H and the 1T' phases. The selection of the substrate and the procedure for the MoTe_2 growth is therefore critical to achieve high quality samples with few grain boundaries, control over both film thickness at the

monolayer level and specific phase formation (in particular the metallic phase), which will determine the final properties of the system.

In this regard, epitaxial graphene on Ir(111) offers several advantages with respect to other substrates. First, it can be easily prepared as a single crystal with a very low defect density. Second, its interaction with TMDs has been demonstrated to be small [29]. Third, graphene exhibits ultra-high mobility and the gate tuneable conductivities, which can improve the properties of the TMDs such as mobility, opening up new opportunities for switching and transport.

In this work, we report on the synthesis and *in situ* characterization of different phases in single-layer MoTe₂ grown on graphene on the (111) face of an iridium single crystal (gr/Ir(111)) by MBE. In particular, the structural and electronic properties of the distinct phases were investigated at the atomic scale by scanning tunneling microscopy (STM). MoTe₂ islands remain decoupled from the substrate due to the weak interaction with graphene, revealing their different electronic nature. We can clearly identify the semiconducting hexagonal phase (1H), the semimetallic distorted octahedral phase (1T') and two other phases resulting from a Te-deficient stoichiometry. Tuning the growth parameters, such as Te:Mo ratio and sample temperature (T_{sample}), we are able to achieve phase engineering in this material and develop a direct synthetic route to produce large areas of pure metallic 1T' phase. Finally, we generate and characterize at the atomic scale different MoTe₂ lateral heterostructures. Our atomic scale investigations constitute an initial step in the understanding of the growth of MoTe₂, a valuable source of knowledge for potential technological applications.

2. Methods

The samples were prepared under ultra-high vacuum (UHV) conditions. The Ir(111) single crystal was initially cleaned by repeated cycles of Ar⁺ sputtering and annealing at 1500 K. Subsequently, the graphene monolayer was grown by exposing the Ir(111) substrate, held at 1400 K, to ethylene at a partial pressure of 1×10^{-7} mbar, to a total dose of 33 L. The crystalline quality of the surface was checked by low energy electron diffraction (LEED) and STM. MoTe₂ films were grown *in situ* by MBE. Elemental Mo (99.9 + % purity) and Te (99.999% purity) were co-evaporated by sublimation from an e-beam evaporator and a Knudsen cell, respectively. Evaporation rates were calibrated on Ir(111) and the Te:Mo ratio was varied in order to get different relative coverage of the phases. As a reference, the deposition rate of Te is 1.9×10^{12} atoms/min·cm² at $T_{\text{Te}}=600$ K and a Mo flux of $\text{Flux}_{\text{Mo}}=20$ nA corresponds to a deposition rate of 1.65×10^{11} atoms/min·cm². The sample temperature (T_{sample}) was kept in the $370 \text{ K} < T_{\text{sample}} < 530 \text{ K}$ range, as controlled by an optical pyrometer with a spectral range of 1.8 - 2.4 μm , mounted in the atmospheric side. While the relative temperature measurements are self consistent within 1 K, the absolute temperature scale might be shifted by up to ± 50 K, due to the uncertainty associated to the radiation lost through the UHV windows. Additionally, post-annealing treatments not longer than 1 hour at the same

growth temperature have been used to improve the epitaxy.

STM experiments were performed *in situ* on two custom-designed UHV systems equipped with low and variable temperature scanning tunneling microscopes, LT-STM and VT-STM, respectively. The base pressure during the experiments was 2×10^{-10} mbar. STM images were recorded in constant current mode and the differential conductance (dI/dV) spectra were taken using a lock-in amplifier ($f = 763.7$ Hz, $V_{pp} = 50$ mV) at 1.2 K. The images were processed using the WSxM [30] and Gwyddion [31] software.

3. Results and Discussion

3.1. Phase engineering

In Figure 1, we examined the evolution of 1H and 1T' coverage as T_{sample} increases under two different deposition rates. A proper MoTe_2 growth requires Te saturation conditions, Te:Mo ratios larger than 10 and temperatures below 500 K (see Supplementary Material section 1 for details of the growth procedure). Under these conditions, the surface is covered with dendritic MoTe_2 islands with irregular edges randomly distributed along the terraces and even crossing step edges, see Fig. 1(a) and (b). This indicates the lack of preferential nucleation centers for the growth, contrary to the growth on bilayer graphene on SiC, where MoTe_2 islands were found to nucleate at graphene steps and then grow along both ascending and descending directions [26]. The height of the islands corresponds to a single layer, see Supplementary Material Fig. S3.

Interestingly, T_{sample} allows the selection of phases with the strongest selectivity being achieved at low temperatures, reaching an almost complete 1T' coverage. This can be seen in Figure 1(d) and (e), which summarize the sample preparations at low deposition rate (one Te cell at $T_{\text{Te}}=600$ K and $\text{Flux}_{\text{Mo}}=20$ nA during 30 minutes) and high deposition rate (three Te cells at $T_{\text{Te}}=610$ K and $\text{Flux}_{\text{Mo}}=150$ nA during 30 minutes), respectively. For a higher partial coverage of the 1H phase, it is necessary low deposition rates and relatively high sample temperatures. In the medium range of sample temperatures both phases coexist, allowing the growth of 1T'/1H heterostructures. Similar results have been reported for MBE growth of MoTe_2 on HOPG [25]. An excess of Te, however, is essential to obtain a stable stoichiometric 2H- MoTe_2 phase by CVD or flux methods [10, 16]. This discrepancy is probably due to the high temperatures used during the CVD and flux growth technique.

Lastly, a rapid drop of the coverage is observed at temperatures above 530 K in both cases. As can be seen in Fig. 1(c), the growth at this temperature results mainly in the formation of elongated structures attributed to the formation of nanowires with a Mo_6Te_6 stoichiometry [32, 33, 34]. We ascribe it to the strong desorption of Te at these high temperatures. A closer view, see inset in Fig. 1(c), shows that the 1D wires stack laterally, forming multiwires without a preferential orientation with respect to the graphene high-symmetry directions. We have also observed the growth of Mo_6Te_6

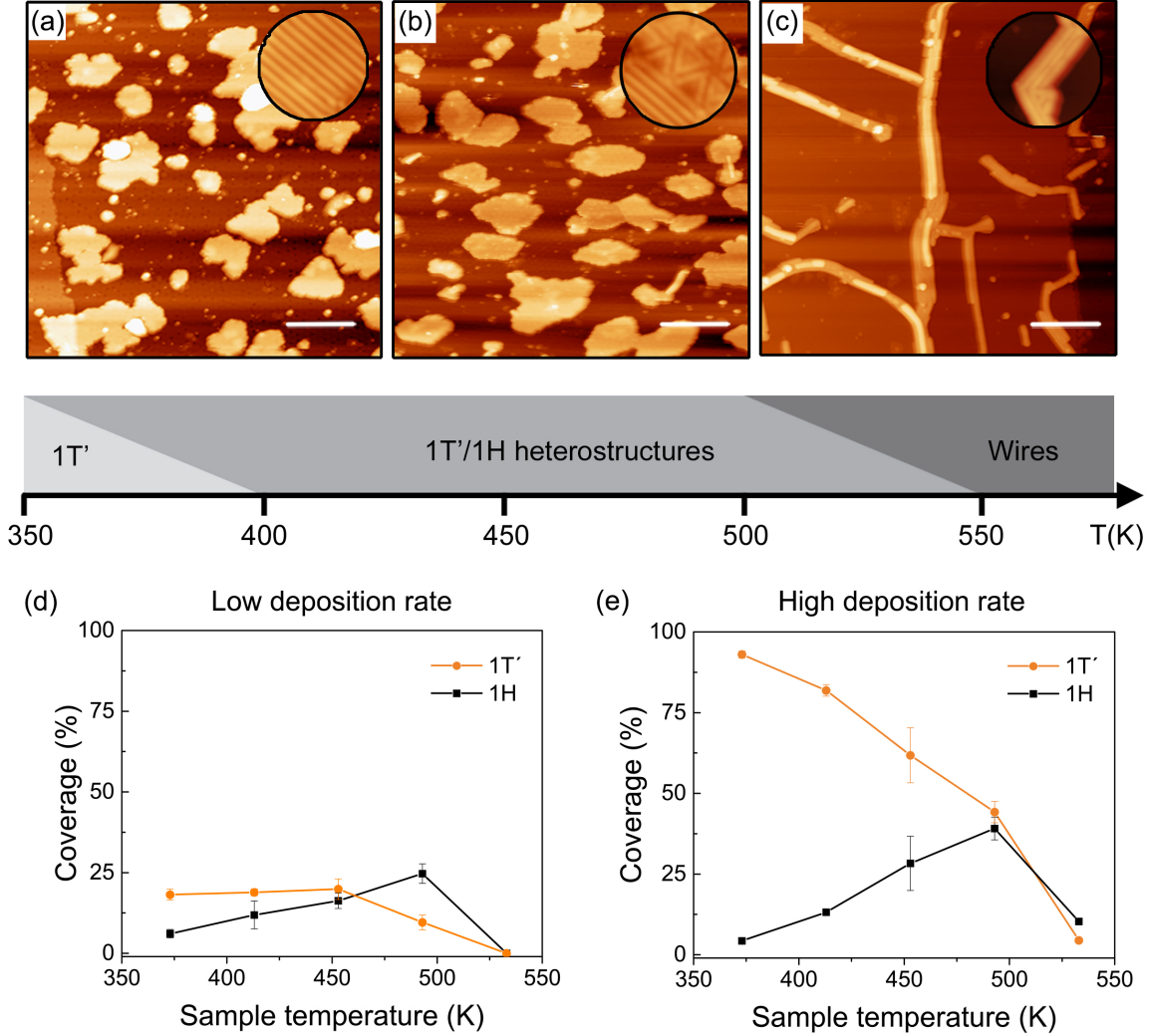


Figure 1: STM images taken at RT after the MoTe₂ growth at (a) $T_{\text{sample}}=370$ K ($V_b = 2$ V and $I_t = 1.3$ nA, scale bar 20 nm), (b) $T_{\text{sample}}=450$ K ($V_b = 2$ V and $I_t = 1.3$ nA, scale bar 20 nm) and (c) $T_{\text{sample}}=530$ K ($V_b = 2.2$ V and $I_t = 0.6$ nA, scale bar 20 nm) for low deposition rate. The inset show the characteristic striped pattern of 1T'-MoTe₂, wagon wheel pattern of MTB areas of 1H-MoTe₂ and a zoom in the Mo₆Te₆ multiwire structure. Coverage of the 1H (black line) and 1T' (orange line) phases as a function of the sample temperature for for 30 minutes deposition at (d) low ($\text{Flux}_{\text{Mo}}=20$ nA and one Te cell at $T_{\text{Te}}=600$ K) and (e) high ($\text{Flux}_{\text{Mo}}=150$ nA and three Te cells at $T_{\text{Te}}=610$ K) deposition rates.

nanowires at low Te:Mo ratio, see Fig.S1(a), which produces the same effect than a MBE growth under Mo-rich conditions. Recently, similar M_6X_6 structures have been reported to undergo a semiconductor-to-metal transition from single to multiwire regime, exhibiting strong Tomonaga-Luttinger liquid characteristics [34, 35].

3.2. Electronic properties

To get an insight of the distinct nature of MoTe₂ phases, we performed scanning tunnelling spectroscopy (STS) at low temperatures. The electronically homogeneous and almost neutral graphene/Ir(111) surface is an ideal playground to explore the electronic properties of MoTe₂ phases.

3.2.1. 1H-MoTe₂ phase We identify the 1H-MoTe₂ phase in STM images by the appearance of linear defects oriented along the three high-symmetry directions (see inset Fig. 1(b) and Fig. 2(a)), known as mirror twin boundaries (MTBs). MTBs appear in most of the 1H-TMDs, being specially abundant in the Mo-TMD family, in particular, in MoTe₂ [36]. Their formation is attributed to three main causes: i) the coalescence during growth of two mirrored domains, ii) accommodation to a slight lack of one of the elements during growth and iii) post-synthesis production by electron irradiation or thermal annealing [36, 37, 38, 39]. In our case, the combination of the six-fold symmetry of graphene and the low efficiency of the growth, which required large Te:Mo ratios during evaporation, results in a high density of MTBs. Their average length is 2.0 ± 0.9 nm, although longer MTBs are often observed, especially at the edge of the islands or domain boundaries, see Fig. 2(a) and Fig. 5(a).

Note also the formation of defect free regions, as can be seen in the left part of the 1H-MoTe₂ island in Fig. 2(a). The hexagonal array of Te atoms in these areas, shown in the inset in Fig. 2(a), has a lattice parameter of 3.45 ± 0.09 Å, in good agreement with the expected value for the 1H-MoTe₂ phase (see Supplementary Material Fig. S4(a)).

In order to identify the electronic properties of this phase, Figure 2(b) shows the dI/dV spectrum taken on a defect free 1H-MoTe₂ area. The phase is obviously a semiconductor with a measured single-particle electronic bandgap of 2.0 ± 0.1 eV. The valence band maximum (VBM) is at -1.25 eV and the conduction band minimum (CBM) at 0.75 eV, which indicates that our 1H-MoTe₂ monolayer is n-doped. This could be due to intrinsic point defects, to a slight Te intercalation underneath graphene or to electron transfer from the more metallic area of the MTBs described above.

The observed electronic gap is almost double of the reported optical gap in multilayer MoTe₂ flakes (1.0-1.3 eV [9, 7, 40, 13]). This is not surprising since, apart from a possible larger optical gap in the 1H-MoTe₂ monolayer, the electronic bandgap is equal to the sum of the optical bandgap and the exciton binding energy, which is expected to be large for 2D-TMDs [41]. The gap observed by tunneling is also larger than the electronic bandgap calculated by conventional density functional theory (DFT) (1.00-1.23 eV [25, 42, 43]), which is widely known to underestimate the value of the quasiparticle gap. However, recently, an alternative G_0W_0 method adapted for calculations of 2D materials provided an energy gap for a free-standing 1H-MoTe₂ layer of $E_{\text{gap}} = 1.9$ eV [8], consistent with our observed value. Finally, it should be mentioned that the slightly different gaps previously measured by STS on a single-layer of MoTe₂ epitaxially grown on HOPG (1.4-1.5 eV [24, 25]) and on BLG/SiC (2.01 eV [27]) may indicate a possible

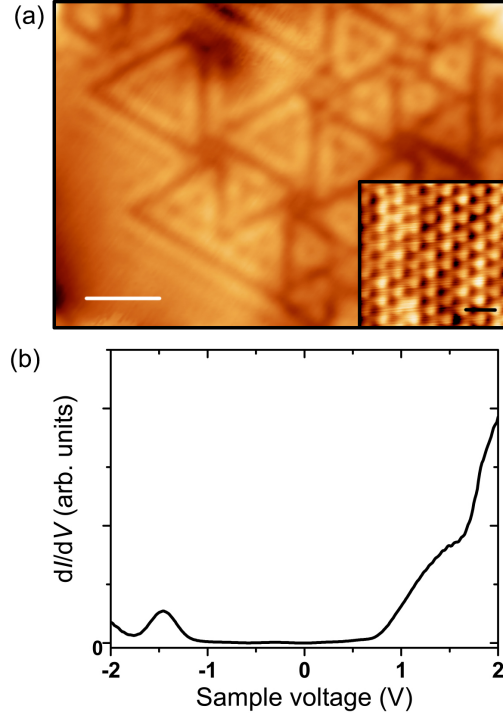


Figure 2: (a) STM image of a 1H-MoTe₂ island with a high density of MTBs ($V_b = 1$ V and $I_t = 0.1$ nA, scale bar 2 nm). The inset shows an atomically resolved image of a defect free area ($V_b = -0.1$ V and $I_t = 0.4$ nA, scale bar 0.6 nm). (b) Average spectrum taken in the left bottom corner of (a) showing the characteristic semiconducting gap of this phase. Measurements were performed at 1.2 K.

dependence of the exciton binding energy on the substrate screening. Indeed, a reduction of 11% in the electronic gap in MoSe₂ grown on HOPG in comparison with the one grown on BLG/SiC has been recently reported [41].

3.2.2. 1T'-MoTe₂ phase The 1T'-MoTe₂ phase is easily recognized by a characteristic striped pattern (see inset of Fig. 1(a) and Fig. 3). These atomic rows are formed by Te atoms on the top layer of MoTe₂ as a consequence of the displacement of the Mo atoms along the a axis of the unit cell, while the Te atoms are staggered along the c axis (see Supplementary Material Fig. S4(b)). The periodicity perpendicular to the stripes is 6.29 ± 0.09 Å, which corresponds to the longer vector of the 1T'-MoTe₂ unit cell. The inset of Fig. 3(a) shows that, at low bias voltages, the two Te rows of the top layer can be atomically resolved, allowing to determine a consistent 1T'-MoTe₂ unit cell with lattice vectors $a = 6.28 \pm 0.05$ Å and $b = 3.32 \pm 0.05$ Å. Notice that the moiré pattern of the gr/Ir(111) substrate is perfectly visible in Fig. 3(a). A close inspection shows that, in this particular case, there is a small misalignment between the gr/Ir(111) and the 1T'-MoTe₂ of $4.8 \pm 0.4^\circ$. However in our samples, we find preferentially three equivalent

rotational orientations of the 1T'-MoTe₂ phase with respect to the substrate, as expected for a two-fold symmetric structure on top of a six-fold symmetric one. The alignment between gr/Ir(111) and 1T'-MoTe₂ is substantially improved after long post-annealing (see Supplementary Material Fig. S5).

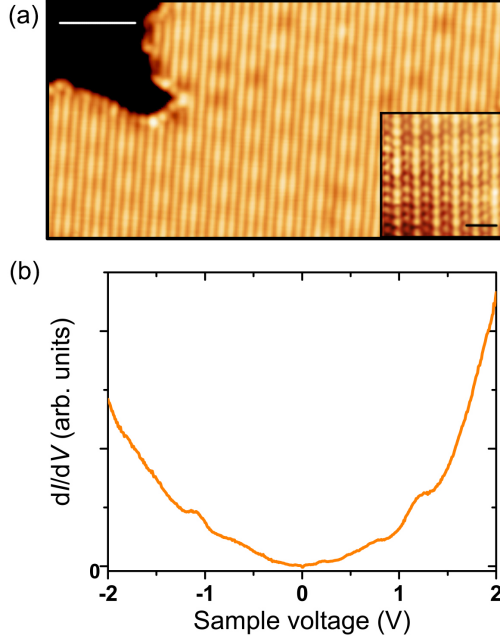


Figure 3: (a) STM image showing a 1T'-MoTe₂ island in which the characteristic stripe pattern can be seen superimposed with the moiré superstructure of the gr/Ir(111) substrate ($V_b = 1$ V and $I_t = 0.1$ nA, scale bar 10 nm). The inset shows an atomically resolved image on one of these areas ($V_b = 0.05$ V and $I_t = 0.1$ nA, scale bar 1 nm). (b) Characteristic dI/dV spectrum showing the semimetallic character of this phase. Data taken at 1.2 K.

The dI/dV spectrum recorded in the 1T' islands shows a semimetallic character with a finite local density of states (LDOS) (Fig. 3(b)) in the gap region of the 1H areas.

3.2.3. $v1H-Mo_5Te_8$ phase In addition to these well-known stable phases of MoTe₂ under Te-deficient conditions, i.e. Te:Mo ratios lower than 10:1, we observe an unexpected structure embedded inside the 1H-MoTe₂ islands, see Fig. 4(a). High-resolution STM images taken in this same region show different hexagonal structures at different bias voltages, see Supplementary Material Fig. S7. Nonetheless, they can be summarized in a large (1.25 ± 0.01 nm) and a small (0.71 ± 0.01 nm) hexagonal periodicity, Fig. 4(b) and (c) respectively.

These structures have intrigued the scientific community in the latest years. At first, the large periodicity was attributed to a moiré pattern resulting of a 30° rotated 1H-MoTe₂ structure on epitaxial graphene [18, 26, 44]. However, this moiré

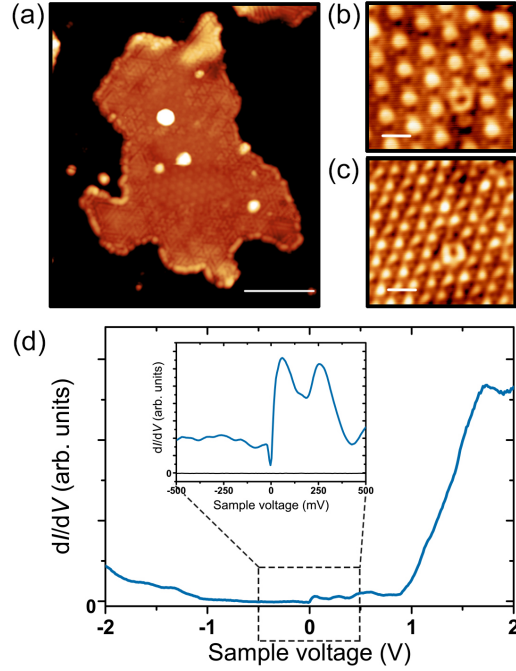


Figure 4: (a) STM image showing a 1H-MoTe₂ island with an embedded large domain of a *v*1H-Mo₅Te₈ phase ($V_b = 1$ V and $I_t = 0.1$ nA, scale bar is 10 nm). (b) Zoom in image on one of these areas taken at 1 V showing a hexagonal pattern with a 1.25 nm periodicity. (c) Same area scanned at -1.1 V, where a different hexagonal pattern with a 0.71 nm periodicity is observed. The defect can be used as a reference. The scale bars of (b) and (c) are 1.2 nm. (d) Characteristic dI/dV spectrum ($V_{\text{mod}}=12.5$ mV) taken on the *v*1H phase. The inset shows a spectrum taken with higher energy resolution in a narrower energy window ($V_{\text{mod}}=5.65$ mV) in which two features can be observed above the Fermi energy. Data were taken at 1.2 K.

superstructure did not explain the different patterns observed. Later, the small periodicity was assigned to the development of a charge density wave (CDW) [24] by the similarities between this structure and those observed on well-studied compounds hosting CDWs, such as 1T-TaS₂ [45] and 1T-TaS_{2-x}Se_x [46]. However, the change of the periodicity with bias voltage in these areas did not support this idea neither. In addition, the STS spectra taken on one of these regions (Fig. 4(d)) reveal new features. At first glance, there is an increase of the LDOS above the Fermi level compared to the 1H spectrum (Fig. 2(b)). Recently, Zhang *et al.* [47] identified these regions as a new polymorphic phase of 2D-MoTe₂ grown by MBE in Te-poor conditions, named *v*1H, with a Mo₅Te₈ stoichiometry belonging to the $P\bar{6}2m$ group, see Fig. S6. This deduction matches our experimental observation that the relative coverage of this phase is promoted in comparison of the others in Mo-rich conditions. A closer look at the STS spectrum (inset in Fig. 4(d) and Fig. S8) reveals two intense features at 50 ± 6 mV and 250 ± 6 mV above the Fermi level and a narrow dip of around 20 mV width at the

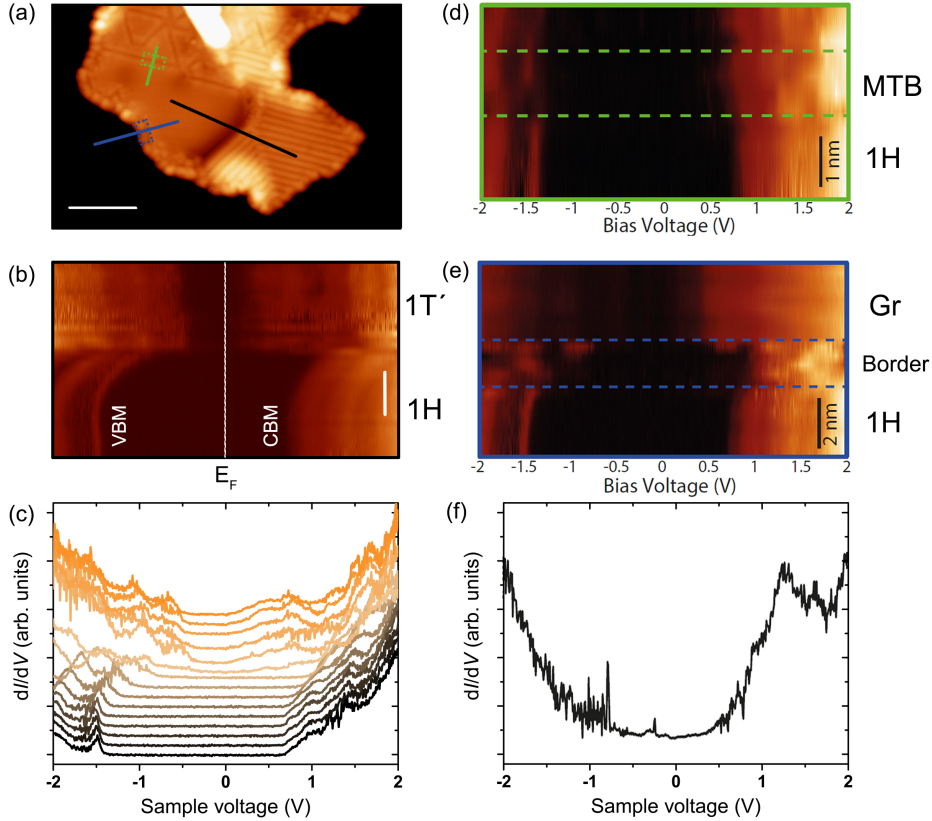


Figure 5: (a) STM image of a MoTe_2 island with different $1\text{T}'/1\text{H}$ interfaces ($V_b = 1\text{ V}$ and $I_t = 0.1\text{ nA}$, scale bar 6 nm). (b) 2D representation (bright color indicates a higher dI/dV signal) and (c) series of dI/dV spectra taken along the black line depicted in (a). (d) 2D representation of the STS taken along the green profile in (a) where no band bending is observed close to MTBs, although gap modifications and gap narrowing are present. (e) 2D plot of the STS measured along the blue profile on (a) where a small upwards band bending ($\sim 0.12\text{ eV}$) occurs. (f) Individual STS extracted from the 1H-MoTe_2 island border marked in (a) where the semiconducting gap is almost vanished. Data were taken at $T=1.2\text{ K}$.

Fermi level. On the one side, two peaks can be identified with relatively flat bands near the Fermi level in agreement with recent DFT calculations [27], as a consequence of the formation of well-ordered MTB. On the other side, a similar narrow dip observed in $1\text{T}'\text{-WTe}_2$ at low temperatures has been attributed to a Coulomb gap due to the electron-electron interaction [48]. These findings are a consequence of the more metallic character of this new phase due to its higher Mo content.

3.3. Interfaces

Interestingly, at growth temperatures below 530 K and above 400 K , we found $1\text{T}'/1\text{H}$ heterostructures. Figure 5(a) shows an island in which these heterostructures with sharp

atomic boundaries are observed.

3.3.1. 1T'/1H interfaces 2D structures combining a semiconductor (1H) and semimetal (1T') have been proposed as a solution to the Schottky contact issue in 2D devices [5, 6, 49]. Even though the fabrication of a 2D device with an ohmic contact has been reported, the control and characterization at the atomic scale of the interface between phases is still lacking. For this purpose, a series of dI/dV spectra were taken along the black line depicted in Fig. 5(a). As can be seen in Fig. 5(c) and in the 2D representation of Fig. 5(b), a rigid shift of 0.5 V towards higher energies in the VBM and CBM of the semiconducting 1H phase is observed. This bending is more pronounced closer to the interface with the 1T' phase and indicates an excess of charge at the semiconducting region. The depletion region extends in a range of around 4 nm and a non-negligible contact resistance can be expected as a consequence of the observed Schottky barrier at the interface, probably induced by the energy band alignment due to the interaction with the substrate.

Similar band bending effects have been reported in other semiconducting TMDs in both lateral and vertical heterojunctions [50, 51, 52], in the vicinity of MTBs and structural defects [53, 54, 55] and at the edges of the material [56, 57].

3.3.2. 1H/MTB interface In contrast, negligible band bending effects are observed at the interfaces between the 1H area and the MTBs region, see the 2D plot of Fig. 5 (d). The absence of a bending is accompanied by the appearance of new in-gap states due to a modulation of the local density of states (LDOS) along the MTB, see Supplementary Information Fig. S9. This modulation has been attributed to an electron confinement along the 1D defects [58]. However, the net charge along the MTB is not enough to induce a band bending in the defect-free 1H region, as has been also reported on MoS₂ [53].

3.3.3. 1H/Graphene interface Finally, we have also explored the boundary between 1H-MoTe₂ and graphene, i.e. the island's edge. In Fig. 5(e), we show the 2D representation of a dI/dV series taken along the blue line depicted in Fig. 5(a) in which a small band bending towards higher energies of ~ 0.12 eV is observed. In addition, at the island's edge, a metallic spectrum is measured, see Fig. 5(f). This metallicity is a consequence of the increase of Mo in these regions, resulting in irregular edges with different stoichiometry. This is common in many semiconducting TMDs due to the easy desorption of chalcogens at the island's edges during growth and has been observed regularly in STM experiments [59, 29]. The smaller band bending in this interface is likely due to the lower work function expected in the graphene compared to 1T' area.

4. Conclusions

We have explored the growth of a single-layer of MoTe_2 on a graphene/Ir(111) substrate. We found that a Te:Mo ratio larger than 10 is required to obtain islands with an appropriate stoichiometry, while T_{sample} allows the control of the relative coverage of the 1H and 1T' phases. In particular, the formation of the 1T' phase is more favorable at low T_{sample} , enabling the fabrication of large areas of this semimetallic phase. Conversely, the growth of the 1H phase is promoted in a Te-deficient atmosphere as T_{sample} rises, resulting in a mix of 1H/1T' phases. For temperatures higher than 530 K, elongated structures with a Mo_6Te_6 stoichiometry are formed.

Each of these phases present different structural and electronic properties at the atomic scale and the low interaction with the graphene allows us to characterize them. The single-layer 1H- MoTe_2 phase on gr/Ir(111) is a semiconductor with an energy bandgap of 2.0 ± 0.1 eV. It presents, however, a high density of MTBs, which have been reported to exhibit a modulation of the charge density providing an ideal platform for exploring collective electron excitations in one-dimensional systems [27, 36]. On the other hand, the 1T' phase presents a semimetallic character. Furthermore, we have seen that Te-poor growth conditions, i.e. low Te:Mo ratio or $T_{\text{sample}} \geq 530\text{K}$, result in the formation of different polymorphs of the layered TMD: Mo_6Te_6 multiwires and a singular $v1\text{H-Mo}_5\text{Te}_8$ structure. The Mo_6Te_6 structures appear in general close to 1H regions and have been reported to be metallic [34, 35]. The hexagonal ($v1\text{H}$) phase presents an uncommon structure belonging to the $P\bar{6}2m$ group and has not been observed so far in other TMDs. This new structure can be produced in large scale under certain conditions [47]. Interestingly, its reduced stoichiometry infers it a metallic character, which can be beneficial for the fabrication of transistors with good electrical contacts [5]. Finally, we use STS to investigate the band-bending at the interfaces between different phases at the atomic scale. In particular, we found a depletion region of around 4 nm corresponding to a local change of the Schottky barrier at the 1H/1T' interface. In conclusion, we have shown a great control of the fabrication of 2D MoTe_2 structures with different electronic properties in a decoupling layer. The possibility to tune and combine these semiconductor (1H) and a semimetal (1T') stable structures even at room temperature opens up a new perspective in the future phase-engineering electronics.

Author Contributions

M.G., A.L.V. and R.M. conceived the idea. A.L.V., F.C. and M.G. planned the experiments. J.R.S., F.C., P.C.A., I.M.I. and M.G. performed the STM experiments and analyzed the data. M.G. and R.M. wrote the manuscript. All authors reviewed and contributed to the manuscript.

Conflicts of interest

There are no conflicts to declare.

Acknowledgements

The authors acknowledge support by the Spanish Ministry of Science and Innovation (Grant no. PGC2018-093291-B-I00, PGC2018-097028-A-I00 and PGC2018-098613-B-C21) and the Comunidad de Madrid (Project S2018/NMT-4511, NMAT2D). IMDEA Nanociencia and IFIMAC acknowledge financial support from the Spanish Ministry of Science and Innovation, through the 'Severo Ochoa' (Grant SEV-2016-0686) and 'María de Maeztu' (Grant CEX2018-000805-M) Programme for Centres of Excellence in R&D, respectively. M.G. has received financial support through the Postdoctoral Junior Leader Fellowship Programme from "la Caixa" Banking Foundation (LCF/BQ/PI18/11630010) and the "Ramón y Cajal" Fellowship program (RYC2020-029317-I).

References

- [1] Lv R, Robinson J A, Schaak R E, Sun D, Sun Y, Mallouk T E and Terrones M 2015 *Accounts of Chemical Research* **48** 56–64
- [2] Wang Q H, Kalantar-Zadeh K, Kis A, Coleman J N and Strano M S 2012 *Nature Nanotechnology* **7** 699–712
- [3] Qian X, Liu J, Fu L and Li J 2014 *Science* **346** 1344–1347
- [4] Lasek K, Li J, Kolekar S, Coelho P M, Guo L, Zhang M, Wang Z and Batzill M 2021 *Surface Science Reports* **76** 100523 ISSN 0167-5729
- [5] Cho S, Kim S, Kim J H, Zhao J, Seok J, Keum D H, Baik J, Choe D h, Chang K J, Suenaga K, Kim S W, Lee Y H and Yang H 2015 *Science* **349** 625
- [6] Guo J and Liu K 2022 *Nanomaterials* **12** 110
- [7] Ruppert C, Aslan O B and Heinz T F 2014 *Nano Letters* **14** 6231–6236
- [8] Rukelj Z and Despoja V 2020 *New Journal of Physics* **22** 063052
- [9] Lezama I G, Ubaldini A, Longobardi M, Giannini E, Renner C, Kuzmenko A B and Morpurgo A F 2014 *2D Materials* **1** 021002
- [10] Keum D H, Cho S, Kim J H, Choe D H, Sung H J, Kan M, Kang H, Hwang J Y, Kim S W, Yang H, Chang K J and Lee Y H 2015 *Nature Physics* **11** 482–486
- [11] Tang Q 2018 *J. Mater. Chem. C* **6**(35) 9561–9568
- [12] Huang H H, Fan X, Singh D J and Zheng W T 2020 *Nanoscale* **12** 1247–1268
- [13] Robert C, Picard R, Lagarde D, Wang G, Echeverry J P, Cadiz F, Renucci P, Högele A, Amand T, Marie X, Gerber I C and Urbaszek B 2016 *Physical Review B* **94** 1–8
- [14] Bae S, Kim H, Lee Y, Xu X, Park J S, Zheng Y, Balakrishnan J, Lei T, Ri Kim H, Song Y I, Kim Y J, Kim K S, Özyilmaz B, Ahn J H, Hong B H and Iijima S 2010 *Nature Nanotechnology* **5** 574–578
- [15] Novoselov K S, Mishchenko A, Carvalho A and Neto A H C 2016 *Science* **353** aac9439
- [16] Park J C, Yun S J, Kim H, Park J H, Chae S H, An S J, Kim J G, Kim S M, Kim K K and Lee Y H 2015 *ACS Nano* **9** 6548–6554
- [17] Zhou J, Liu F, Lin J, Huang X, Xia J, Zhang B, Zeng Q, Wang H, Zhu C, Niu L, Wang X, Fu W, Yu P, Chang T R, Hsu C H, Wu D, Jeng H T, Huang Y, Lin H, Shen Z, Yang C, Lu L, Suenaga K, Zhou W, Pantelides S T, Liu G and Liu Z 2017 *Advanced Materials* **29** 1603471

- [18] Pham T T, Castelino R, Felten A and Sporcken R 2020 *Applied Surface Science* **523** 1–10
- [19] He Q, Li P, Wu Z, Yuan B, Luo Z, Yang W, Liu J, Cao G, Zhang W, Shen Y, Zhang P, Liu S, Shao G and Yao Z 2019 *Advanced Materials* **31** 1–11
- [20] Ogorzalek Z, Seredynski B, Kret S, Kwiatkowski A, Korona K P, Grzeszczyk M, Mierzejewski J, Wasik D, Pacuski W, Sadowski J and Gryglas-Borysiewicz M 2020 *Nanoscale* **12** 16535–16542 ISSN 20403372
- [21] Vishwanath S, Sundar A, Liu X, Azcatl A, Lochocki E, Woll A R, Rouvimov S, Hwang W S, Lu N, Peng X, Lien H H, Weisenberger J, McDonnell S, Kim M J, Dobrowolska M, Furdyna J K, Shen K, Wallace R M, Jena D and Xing H G 2018 *Journal of Crystal Growth* **482** 61–69
- [22] Tsipas P, Fragkos S, Tsoutsou D, Alvarez C, Sant R, Renaud G, Okuno H and Dimoulas A 2018 *Advanced Functional Materials* **28** 1–12 ISSN 16163028
- [23] Roy A, Movva H C P, Satpati B, Kim K, Dey R, Rai A, Pramanik T, Guchhait S, Tutuc E and Banerjee S K 2016 *ACS Applied Materials & Interfaces* **8** 7396–7402
- [24] Dong L, Wang G Y, Zhu Z, Zhao C X, Yang X Y, Li A M, Chen J L, Guan D D, Li Y Y, Zheng H, Xie M H and Jia J F 2018 *Chinese Physics Letters* **35** 066801
- [25] Chen J, Wang G, Tang Y, Tian H, Xu J, Dai X, Xu H, Jia J, Ho W and Xie M 2017 *ACS Nano* **11** 3282–3288
- [26] Yu Y, Wang G, Qin S, Wu N, Wang Z, He K and Zhang X A 2017 *Carbon* **115** 526–531
- [27] Wang L, Wu Y, Yu Y, Chen A, Li H, Ren W, Lu S, Ding S, Yang H, Xue Q K, Li F S and Wang G 2020 *ACS Nano* **14** 8299–8306
- [28] Diaz H C, Chaghi R, Ma Y and Batzill M 2015 *2D Materials* **2** 044010
- [29] Hall J, Pielic B, Murray C, Jolie W, Wekking T, Busse C, Kralj M and Michely T 2018 *2D Materials* **5** 025005
- [30] Horcas I, Fernández R, Gómez-Rodríguez J M, Colchero J, Gómez-Herrero J and Baro A M 2007 *Review of Scientific Instruments* **78** 013705
- [31] Nečas D and Klapetek P 2012 *Central European Journal of Physics* **10** 181–188
- [32] Yu Y, Wang G, Tan Y, Wu N, Zhang X A and Qin S 2018 *Nano Letters* **18** 675–681
- [33] Zhu H, Wang Q, Zhang C, Addou R, Cho K, Wallace R M and Kim M J 2017 *Advanced Materials* **29** 1606264
- [34] Deng J, Huo D, Bai Y, Guo Y, Pan Z, Lu S, Cui P, Zhang Z and Zhang C 2020 *Nano Letters* **20** 8866–8873
- [35] Xia Y, Wang B, Zhang J, Jin Y, Tian H, Ho W, Xu H, Jin C and Xie M 2020 *Nano Letters* **20** 2094–2099
- [36] Batzill M 2018 *Journal of Physics Condensed Matter* **30** 493001
- [37] Komsa H P and Krasheninnikov A V 2017 *Advanced Electronic Materials* **3** 1–10
- [38] Coelho P M, Komsa H P, Coy Diaz H, Ma Y, Krasheninnikov A V and Batzill M 2018 *ACS Nano* **12** 3975–3984
- [39] Diaz H C, Ma Y, Chaghi R and Batzill M 2016 *Applied Physics Letters* **108** 191606 ISSN 0003-6951 URL <http://aip.scitation.org/doi/10.1063/1.4949559>
- [40] Lezama I G, Arora A, Ubaldini A, Barreateau C, Giannini E, Potemski M and Morpurgo A F 2015 *NanoLetters* **15** 2336
- [41] Ugeda M M, Bradley A J, Shi S F, Da Jornada F H, Zhang Y, Qiu D Y, Ruan W, Mo S K, Hussain Z, Shen Z X, Wang F, Louie S G and Crommie M F 2014 *Nature Materials* **13** 1091–1095
- [42] Kumar A and Ahluwalia P K 2012 *European Physical Journal B* **85** 18–22
- [43] Kan M, Nam H G, Lee Y H and Sun Q 2015 *Physical Chemistry Chemical Physics* **17** 14866–14871
- [44] Castelino R, Pham T T, Felten A and Sporcken R 2020 *Nanotechnology* **31** 115702
- [45] Cho D, Cho Y H, Cheong S W, Kim K S and Yeom H W 2015 *Physical Review B - Condensed Matter and Materials Physics* **92** 1–5
- [46] Qiao S, Li X, Wang N, Ruan W, Ye C, Cai P, Hao Z, Yao H, Chen X, Wu J, Wang Y and Liu Z 2017 *Physical Review X* **7** 1–10
- [47] Zhang J, Xia Y, Wang B, Jin Y, Tian H, kin Ho W, Xu H, Jin C and Xie M 2020 *2D Materials*

8 015006

- [48] Song Y H, Jia Z Y, Zhang D, Zhu X Y, Shi Z Q, Wang H, Zhu L, Yuan Q Q, Zhang H, Xing D Y and Li S C 2018 *Nature Communications* **9** 4071
- [49] Zheng Y, Gao J, Han C and Chen W 2021 *Cell Reports Physical Science* **2** 100298
- [50] Ou Y, Kang Z, Liao Q, Zhang Z and Zhang Y 2020 *Nano Research* **13** 701–708
- [51] Kobayashi Y, Yoshida S, Sakurada R, Takashima K, Yamamoto T, Saito T, Konabe S, Taniguchi T, Watanabe K, Maniwa Y, Takeuchi O, Shigekawa H and Miyata Y 2016 *Scientific Reports* **6** 1–8
- [52] Taghinejad H, Eftekhar A A and Adibi A 2019 *Optical Materials Express* **9** 1590
- [53] Murray C, Van Efferen C, Jolie W, Fischer J A, Hall J, Rosch A, Krasheninnikov A V, Komsa H P and Michely T 2020 *ACS Nano* **14** 9176–9187
- [54] Liu X, Balla I, Bergeron H and Hersam M C 2016 *Journal of Physical Chemistry C* **120** 20798–20805
- [55] Yan C, Dong X, Li C H and Li L 2018 *Nanotechnology* **29** 195704
- [56] Zhang C, Johnson A, Hsu C L, Li L J and Shih C K 2014 *Nano Letters* **14** 2443–2447
- [57] Quang T L, Nogajewski K, Potemski M, Dau M T, Jamet M, Mallet P and Veuillen J Y 2018 *2D Materials* **5** 035034
- [58] Jolie W, Murray C, Weiß P S, Hall J, Portner F, Atodiresei N, Krasheninnikov A V, Busse C, Komsa H P, Rosch A and Michely T 2019 *Physical Review X* **9** 11055 ISSN 21603308
- [59] Bollinger M V, Lauritsen J V, Jacobsen K W, Nørskov J K, Helveg S and Besenbacher F 2001 *Physical Review Letters* **87** 3–6